OPEN ACCESS
Journal of Innovative Optical Health Sciences
Vol. 16, No. 3 (2023) 2250036 (12 pages)

DOI: 10.1142/S1793545822500365

World Scientific
www.worldscientific.com

Research on the detection of early caries based on hyperspectral imaging

Cheng Wang*,¶, Haoying Zhang*, Guangyun Lai†, Songzhu Hu‡, Jun Wang† and Dawei Zhang§

*Institute of Biomedical Optics and Optometry
Key Laboratory of Medical Optical Technology and
Instruments Ministry of Education
University of Shanghai for Science & Technology, 200093, P. R. China

†Department of Paediatric Dentistry, Ninth People's Hospital
Shanghai Jiaotong University, 200011, P. R. China

‡Equipment Department
Nantong Hospital of Traditional Chinese Medicine
226007, P. R. China

§Engineering Research Centre for Optical Instruments and Systems
Ministry of Education, Shanghai Key Laboratory of
Modern Optical Systems, University of Shanghai for
Science & Technology, 200093, P. R. China
¶c.wang@usst.edu.cn

Received 8 May 2022
Accepted 24 August 2022
Published 28 November 2022

Objective: We applied hyperspectral imaging (HSI) system to distinguish early caries from sound and pigmented areas. It will provide a theoretical basis and technical support, for research and development of an instrument that could be used for screening and detection of early dental caries.

Methods: Eighteen extracted human teeth (molars and premolars), with varying degrees of natural pathology and no degree of decay involving dentin were obtained. HSI system with a wavelength range from 400 to 1000 nm was used to obtain images of all 18 teeth containing sound, carious and pigmented areas. We compared the spectra of the wavebands at both 500 nm and 780 nm from the different tooth states, and the reflectance difference between sound versus carious lesions and sound versus pigmented areas, respectively.

Results: There was a slight difference in reflectance between carious areas and pigmented areas at 500 nm. A substantial difference was additionally noted in reflectance between carious areas and pigmented areas at 780 nm.

Conclusion: The results have shown that the interference of tooth surface pigment can be eliminated in the near-infrared (NIR) waveband, and the caries can be effectively identified from the

pigmented areas. Thus, it could be used to detect carious areas of teeth in place of the traditional visual inspection method or white light endoscopy.
Clinical significance: The NIR diffused light signal enables the identification of early caries from pigment and other interference, providing a reasonable detection tool for early detection and early treatment of teeth diseases.

Keywords: Hyperspectral imaging; near-infrared light; early dental caries; spectral reflectance.

1. Introduction

Caries is a common oral disease. At present, visual inspection and dental radiography still are conventional caries detection methods. It is easy, however, to miss the early stages of caries by failing to identify hyperpigmentation, because the color of the pigmented areas is similar to that of early caries under the visible light; with these methods, especially the occult caries on the adjacent side of the teeth, which can facilitate tooth decay from a lighter dental caries. In addition, dental radiography is associated with ionizing radiation and should not be performed more than once in a short period of time, especially in the case of children.[1–4] Furthermore, it is apparent that during the examination, pigmentation and caries on the tooth surface are usually found at the same time due to long-term poor use or irregular cleaning. This leads some doctors to misdiagnose early caries as tooth surface pigmentation too easily, also resulting in untimely treatment or inappropriate treatment by mistaking tooth surface pigmentation for early caries.

Hyperspectral imaging (HSI) is an emerging imaging modality for medical applications, especially in disease diagnosis and image-guided surgery.[5] An HSI system is mainly composed of the light source, wavelength dispersion devices, and two-dimensional (2D) detector array. There are three main spectral imaging methods, including point-scan, line-scan (pushbroom), and plane scan(snapshot) according to the way the hyperspectral data are obtained. Point-scan HSI systems are often identified with spectrophotometers equipped with probes for illuminating a small local area from the object and for perception of the reflected, transmitted or absorbed light. It requires two degrees of freedom in both directions. Line-scan HSI systems obtain spectral imaging data of one pixel row at a time. Snapshot HSI systems obtain spectral characteristics in all pixels in the image got from the hyperspectral camera. It is currently used to achieve spectral imaging data through multi-channel filters. The image is fast, but the spectral resolution is low. This paper used pushbroom HSI system, its basic principle is that a sample, illuminated by a light source, is projected through an optical lens system into a monochromator, and a series of narrow spectral bands of light are then focused onto a 2D detector array. In other words, these narrow spectral band lights were focused onto a camera sequentially. By collecting spectral information at each pixel of a 2D detector array, HSI generates a three-dimensional (3D) dataset of spatial and spectral information, known as a hypercube. The principle of an HSI system is shown in Fig. 1.

An emerging HSI modality is an effective, noninvasive optical imaging technique that can overcome the shortcomings of other traditional imaging techniques. Moreover, it can obtain not only high-resolution two dimensions spatial images, but also

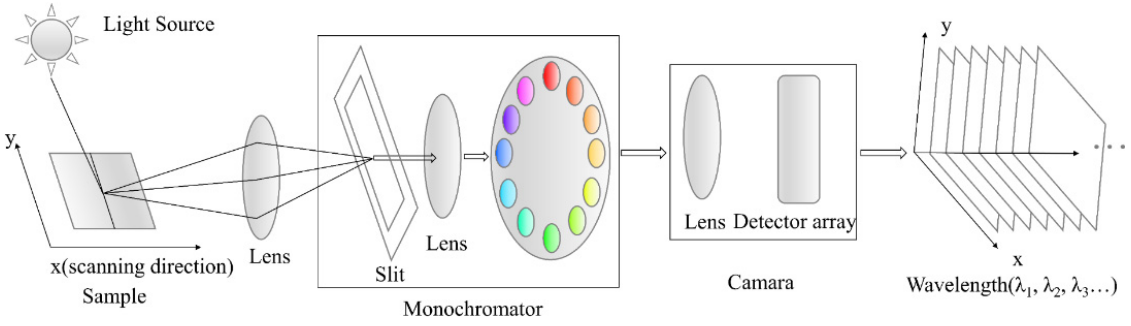

Fig. 1. Schematic diagram of a HSI system.

spectral dimension information, and it has been used in remote sensing, food testing, biomedical imaging, and other technical fields.[6–8]

In the oral health field, dental caries is the most prevalent form of oral diseases. The applications of HSI technology in the detection of dental caries *in vitro* are mainly as follows: A NIR hyperspectral camera was used to analyze the reflection spectrum of the teeth, combined with different algorithms to quantify the severity of the lesions, and to evaluate the accuracy of the quantification criteria. For example, Usenik *et al.* used an NIR HSI system to image the water from artificial and natural carious tooth enamel samples.[9] Partial least squares regression analyzed based on the spectra imaging was used to predict the water content of the samples. By modeling the process of water evaporation from enamel surfaces, the applicability of water evaporation kinetics in healthy and demineralized enamel was assessed in the detection and quantification of initial caries using NIR HSI. El-Sharkawy *et al.* used a helium–neon (He–Ne) laser source with the wavelength of 633 nm and the power of 5 mW, to irradiate human tooth samples, and obtained reflection and emission spectra with the hyperspectral cameras.[10] The chemical footprint characteristics of each tooth element and caries state were obtained in the characteristic spectrum of the tooth tissue, which can be used to diagnose and classify different types and stages of dental caries. Both enamel and dentin caries can be distinguished under the 633 nm illumination spectral profile, and white spot lesions could be clearly detected and identified in the far visible and infrared waveband ranges.

On the other hand, the hardware unit of the NIR HSI system was used to improve the quality of imaging of the tooth. For example, El-Sharkawy *et al.* investigated a customized optical imaging system based on an HSI technique, which could provide high sensitivity, high resolution and early caries detection.[11] Abdel Gawad *et al.* designed a fluorescence HSI system, using a laser diode with a wavelength of 395 nm as the excitation light source.[12] The images of 12 teeth obtained were displayed and processed using HSAnalysis2XL, which is a customized digital and image signal processing algorithms, and searched a set of wavelengths that can be used to diagnose leukoplakia, root calculus, enamel, and dentin caries.

With the development of HSI technology, many scholars have applied HSI in other oral diseases. For example, Chang *et al.* compared the principal component score results based on the spectral features of the images for different levels of periodontal disease and identified staging periodontal disease, according to the variation trend of spectral features.[13] Wang *et al.* used multi-spectral imaging (MSI) with color reproduction systems to visualize oral tissues and improve the efficiency of medical diagnosis of oral cancer.[14] Moreover, Daniel *et al.* combined HSI with deep learning, in order to distinguish human-oral fat, muscle and oral mucosa.[15] Urban *et al.* built a multimodal, HSI system termed Hyperspectral-Fluorescence-Spatial Frequency Domain Imaging (Hy-F-SFDI), used to quantify gingival tissue hemoglobin volume fraction, detect caries and bacterial activity, and measure tooth color of a volunteer at different time points.[16] Wang *et al.* combined MSI with color reproduction technique to obtain the optimal lighting for oral cavity detection.[17]

Based on previous studies, it has been found that most studies used NIR HSI system to improve the classification accuracy of dental caries and realize automatic classification. The majority, however, ignored the effect of pigments attached to the tooth surface on the detection of early dental caries. It is hard to distinguish pigments and early dental caries directly by the naked eye. The objective of this paper therefore, is to use the HSI system in the range of 400–1000 nm to obtain some images, and subsequently to find a waveband that is specific for early caries, to distinguish the sound, carious, and pigmented areas of the teeth, so as to identify early dental caries from pigmentation and other disturbances. This would then provide a theoretical basis, coupled with technical support, for future research and development of an instrument that could diagnose early dental caries.

2. Materials and Methods

2.1. *Sample preparation and sampling instruments*

Eighteen extracted human teeth (molars and premolars) with varying degrees of natural pathology and no degree of decay involving dentin were obtained from the Department of Dentistry, Ninth People's Hospital, the Shanghai Jiaotong University. The isolated teeth were cleaned, the soft tissue was removed, and they were stored in a separate

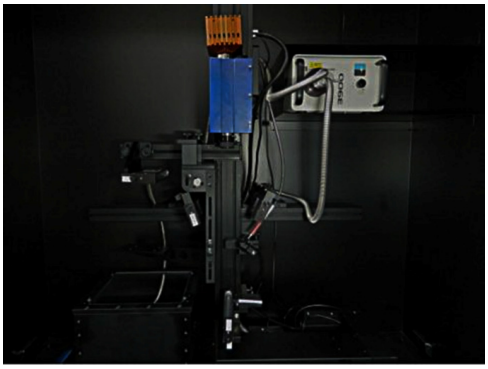

Fig. 2. HSI system.

container of 0.9% sodium chloride solution, in order to maintain sufficient moisture and aseptic environment. Any excess moisture was removed by wiping lightly with a cotton swab when the sample images were taken.

A push-scan visible-near infrared HSI system (HSI-VNIR-B1621, ISUZU OPTICS, Taiwan, China) is used to collect hyperspectral images, as shown in Fig. 2. The system has a spectral range of 400–1000 nm, a spectral resolution of 0.64 nm, an exposure time of 6.8 ms, and a spatial resolution of $< 9\,\mu$m.

2.2. *Radiation correction of instrument*

In this study, the method of reference whiteboard correction is used to convert the meaningless DN values to reflectance values $R(\lambda)$.

The spectral response of the system was characterized by acquiring images $\mathrm{DN}_w(\lambda)$ of a standard diffuse ceramic, while the dark response was characterized by acquiring an image $\mathrm{DN}_{\mathrm{dark}}(\lambda)$ when the light source was turned off and the lens was completely covered by a nonreflective opaque black cap. The acquired images $\mathrm{DN}_{\mathrm{sample}}(\lambda)$ were preprocessed according to the following equation[1]:

$$R(\lambda) = \frac{\mathrm{DN}_{\mathrm{sample}}(\lambda) - \mathrm{DN}_{\mathrm{dark}}(\lambda)}{\mathrm{DN}_w(\lambda) - \mathrm{DN}_{\mathrm{dark}}(\lambda)} \times R_w(\lambda), \quad (1)$$

where $R_w(\lambda)$ is the spectral reflectance ratio of the standard whiteboard, Fig. 3 shows the spectra before and after radiation correction.

2.3. *Image preprocess and analysis*

Limited by the push-scan acquisition method of the hyper-spectrometer, the background accounts for a high proportion of the original image. So first, the image is cropped according to the size of the tooth, and all the band data is retained. In the process of acquiring and transmitting hyperspectral image data, the imperfection of imaging system, transmission medium and equipment and improper image processing, will generate noise, thus affecting the visual effect and aesthetics of the image, in addition to the feature extraction and information analysis in subsequent processing.[16] Each acquired hyperspectral cube consisted of 955 spectral images covering the spectral range from 400 nm to 1000 nm with spectral resolution of 0.64 nm.

Second, the noise of the cropped image is reduced. In order to effectively reduce the noise of the hyperspectral images, it was necessary to identify the type of noise from the outlet. In this study, a small area of the tooth, as monochromatic as possible, was selected. The grayscale histogram of this area was then obtained, which can better represent the noise characteristics of the image.

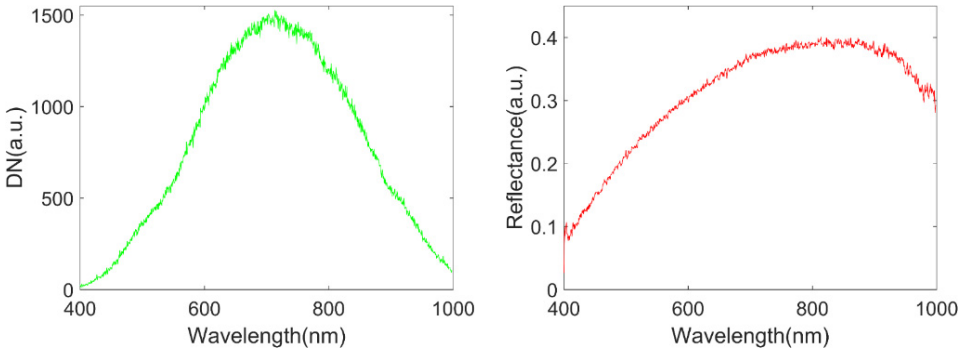

(a) (b)

Fig. 3. Spectra before and after radiation correction, where (a) is the figure of DN before radiation correction, (b) is the figure of reflectance after radiation correction.

Finally, the full band spectral information of different parts is further analyzed from the spectral dimension, in order to identify early caries from pigment and other interference. The analysis process is realized on ENVI 5.3 software (Exelis VIS, USA).

3. Results

3.1. *Hyperspectral image*

There are 54 regions of interest in 18 teeth, including healthy areas, carious areas and tooth surface pigmentation. Severe dental caries and repaired tooth surfaces are excluded from this study. After fixation of the teeth for HSI, the obtained hyperspectral images were radiometrically corrected and the image is denoised to compensate for the spectral response of the system and the dark current of the camera, and to improve the image and spectral quality.

The cube data of hyperspectral images of a tooth acquired with HSI system are shown in Fig. 4 with every other 40 nm. These images contain not only the spatial information of the teeth, but also the spectral data arising from each point on the image. Figure 4 shows the hyperspectral image information collected for every other 40 nm.

3.2. *Image denoising*

Three of the teeth were taken as examples. The gray histogram of the selected area on the three teeth in Figs. 5(a), 5(c), and 5(e) is shown in Figs. 5(b), 5(d), and 5(f), respectively. According to the grayscale histogram, we find that it belongs to a normal distribution. Normally distributed noise is termed as Gaussian noise. For Gaussian noise, the mean filtering method could be used to denoise the images. In the spectral image, each pixel point contains its corresponding spectrum. In this study, a pixel corresponding to the red dot position in Fig. 5 was randomly selected from the three teeth, shown in Figs. 6(a)–6(c). The pixels with the coordinates (787,461), (720,514), and (715,311) on the three teeth were selected, respectively. Comparing the spectral reflectance before and after the denoising process (Fig. 6), the mean filtering obtained a better effect for the noise reduction.

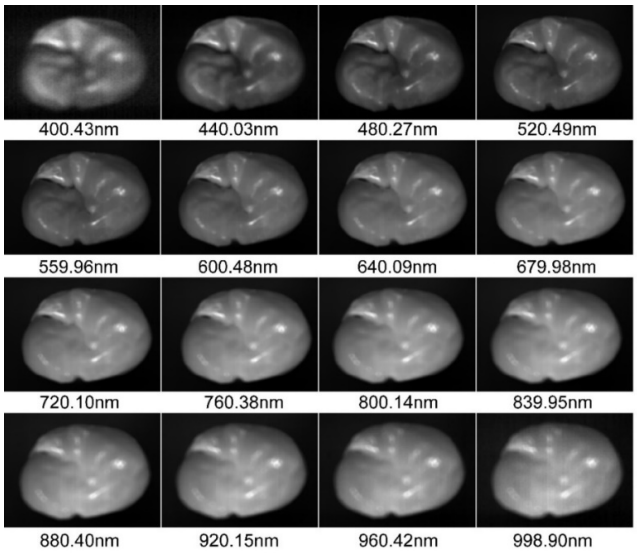

Fig. 4. Hyperspectral image of a tooth.

3.3. *Spectral analysis*

First of all, the different regions of interest of the same tooth were analyzed, including sound areas, carious areas, and pigmented areas. As shown in Figs. 7(a)–7(d), the spectra of 45 pixels (within the region of interest) were randomly selected. The spectral reflectance of the pigmented areas is similar to the early carious areas in visible wavebands (500 ± 50 nm). Moreover, in NIR wavebands (830 ± 70 nm), the spectral reflectance of the sound states is similar to the pigmented areas, while the spectral reflectance of carious states is much lower than that of the sound and pigmented areas.

Therefore, in order to understand more clearly the spectrum differences between the carious, the sound and pigmented states, a block with pixels of 4×4 was selected from the sound, pigmented, and early carious areas of interest, respectively, and the mean reflectance values were calculated. Figure 8(a) illustrates the tooth images acquired by the hyper spectrometer, with the red, green, and blue arrows pointing to the 4×4 sized carious, sound and pigmented surfaces, respectively. In addition, Fig. 8(b) shows a comparison of the mean values of reflectance of the three areas selected from the teeth in Fig. 8(a). Selecting representative wavebands (500 nm and 780 nm) from 18 teeth quantified the spectral reflectance of carious, sound, and pigmented surfaces at 500 nm and 780 nm (Fig. 9), and there was a slight difference in reflectance between carious areas and pigmented areas at 500 nm, for example in teeth 11 and 16. There was also a large difference in reflectance between carious areas and pigmented areas at 780 nm, such as tooth 1, tooth 2,

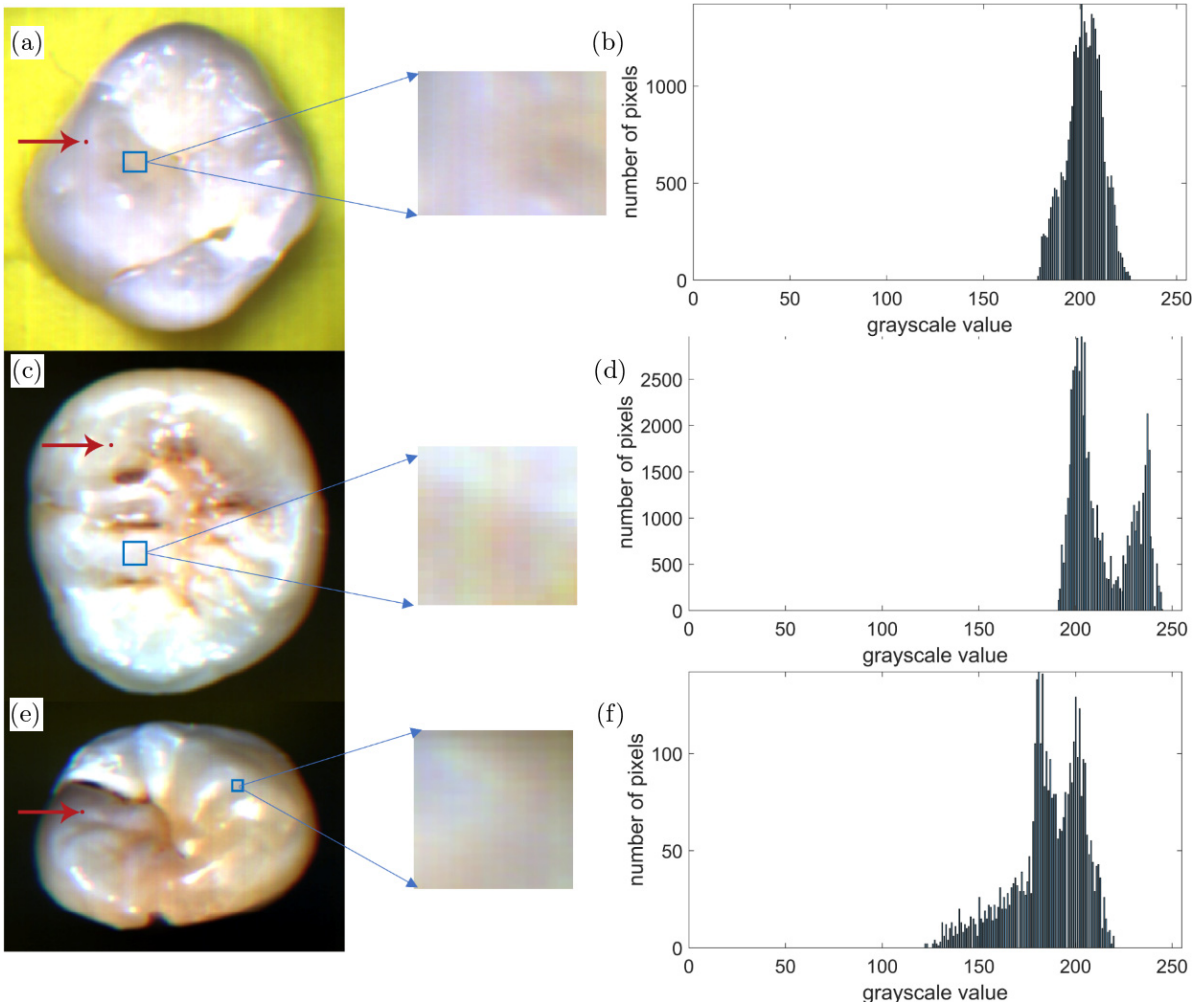

Fig. 5. Noise-type identification, where (b), (d), and (f) are the grayscale histograms in the blue boxes in (a), (c), and (e), respectively.

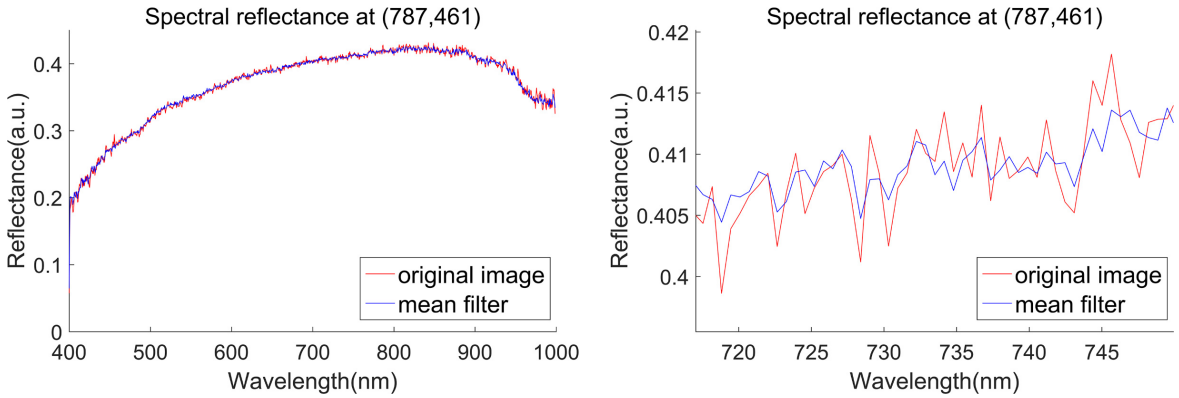

(a) (b)

Fig. 6. Comparison of spectral reflectance between the original images and denoising images, where Fig. 6(a) is the reflection spectrum of tooth a at pixel point (787,461), Fig. 6(c) is the reflection spectrum of tooth c at pixel point (720,514), Fig. 6(e) is the reflection spectrum of tooth e at pixel point (715,311), (b), (d) and (f) is (a), (c) and (e) region magnification, respectively.

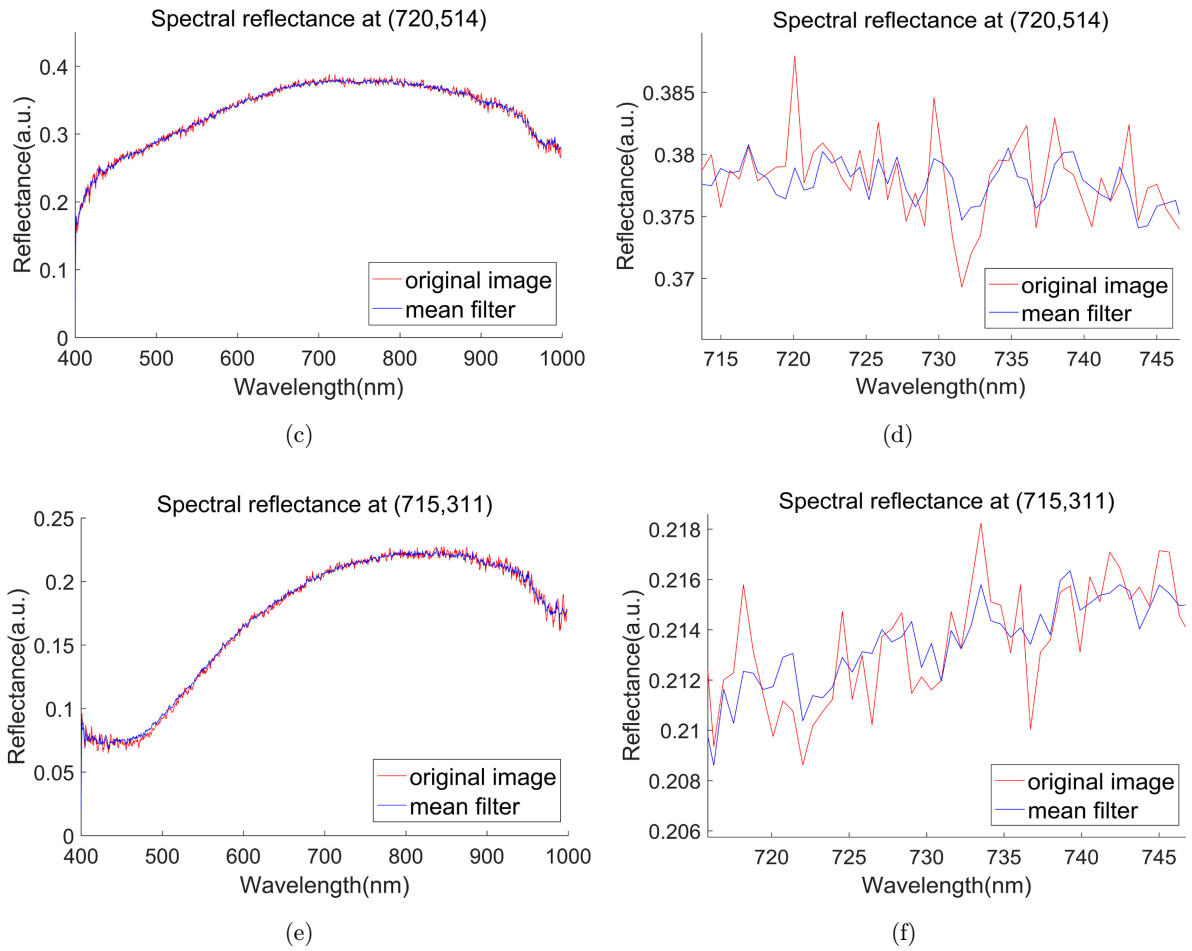

Fig. 6. (*Continued*)

tooth 14, and so on. Therefore, carious lesions could be distinguished from healthy and pigmented areas in the NIR waveband.

Finally, the spatial information of each waveband in the original image was taken, including both the visible wavebands and the NIR wavebands, and then the spatial images of the different wavebands were analyzed complaisantly. As shown in Figs. 10(a) and 10(c), the black spots in the hyperspectral image of the tooth at 500 nm wavebands, pointed by a red arrow and a green arrow, were the same obvious. As shown in Figs. 10(b)

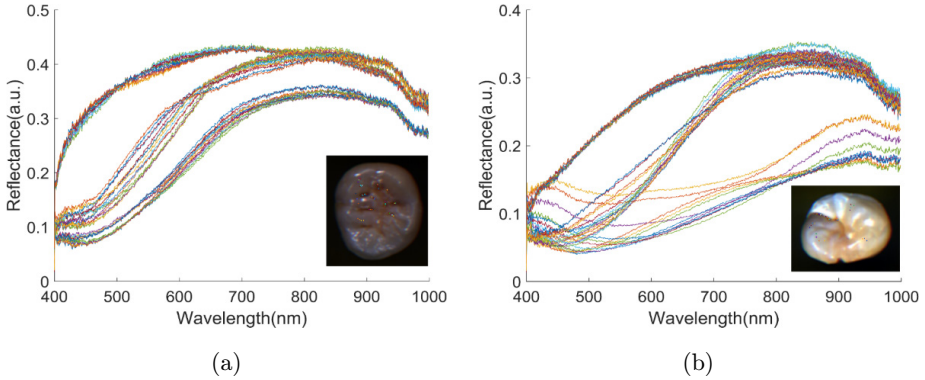

Fig. 7. The spectral reflectance of 45 randomly pixels from 4 teeth.

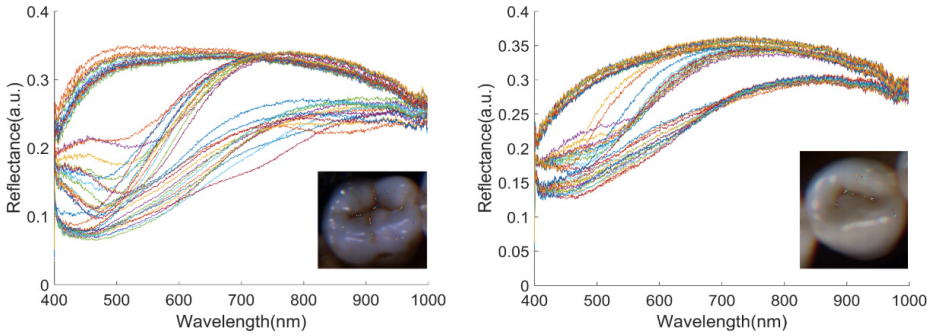

(c) (d)

Fig. 7. (*Continued*)

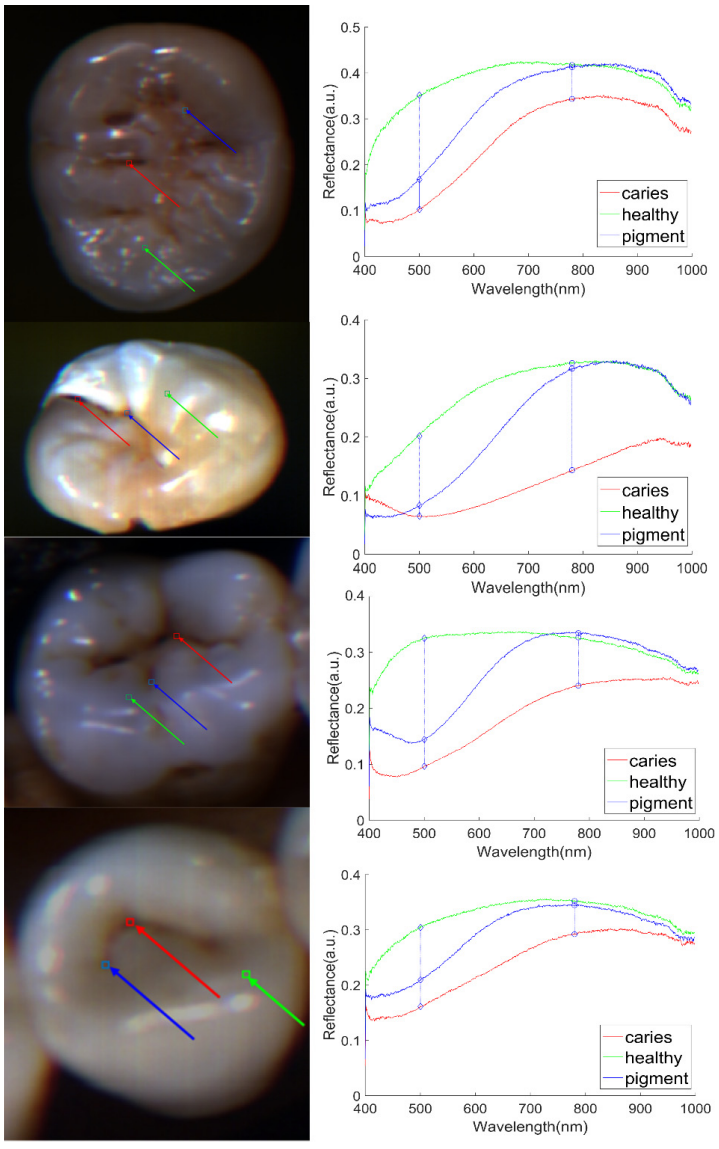

(a) (b)

Fig. 8. Average spectral reflectance of teeth, where (a) is the teeth, the carious areas pointed with red arrows, the sound areas pointed with green arrows, and the pigmented areas pointed with blue arrows, and (b) is the spectral reflectance curves in (a).

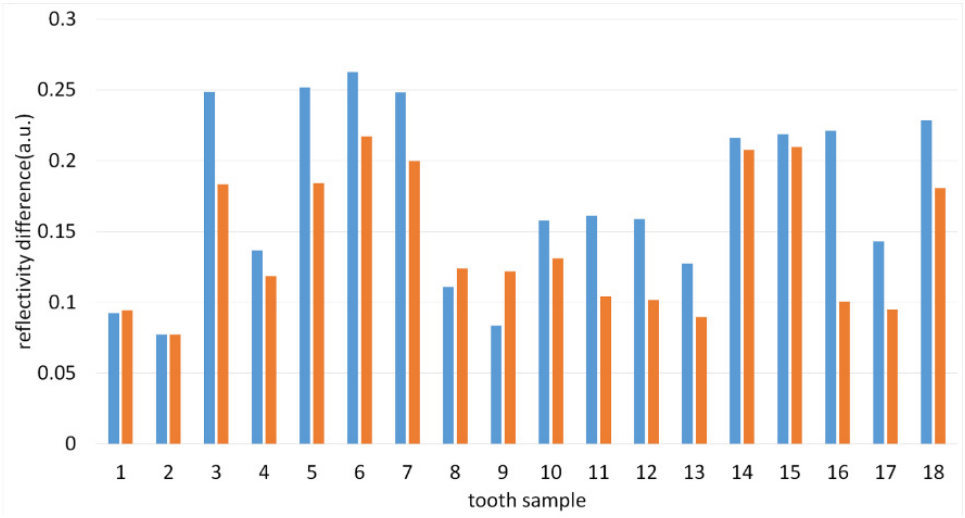

(a)

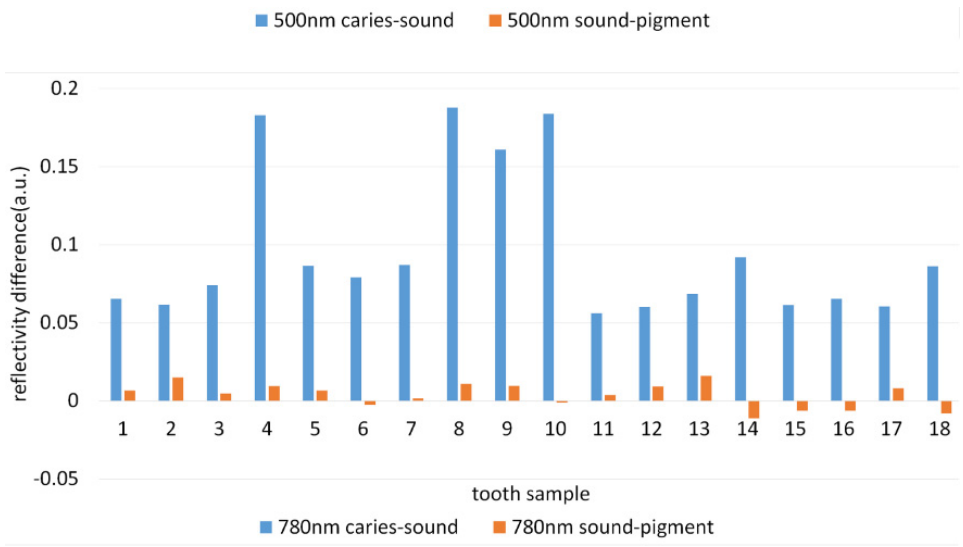

(b)

Fig. 9. Comparison of the spectral reflectance differences of teeth at 500 nm and 780 nm, where (a) is the comparison of the spectral reflectance difference between sound-carious versus sound-pigmented at 500 nm and (b) is a comparison of the spectral reflectance difference between sound-carious versus sound-pigmented at 780 nm.

and 10(d), the black spots in the spatial image of the tooth at 780 nm wavebands, pointed by a red arrow, have disappeared, albeit with a black dark shadow still remaining, as pointed by the green arrows.

In summary, HSI technique can solve the problems encountered in early caries detection associated with the influence of pigmentation on caries detection, through the analysis of spectral curves in different tooth states, especially in the NIR wavebands. This can not only better identify caries from healthy teeth, but also better distinguish caries from pigmentation interference, and improve the reliability of caries diagnosis.

4. Discussion and Conclusion

In order to identify the early caries from pigmented areas, teeth with a caries index of 0–2, based on the International Caries Detection and Assessment System (ICDAS) II standard, were studied[18] Early caries are invasive to enamel but not to dentin. The spectra of the multiple carious surfaces were similar, but they were different from the pigmented surfaces

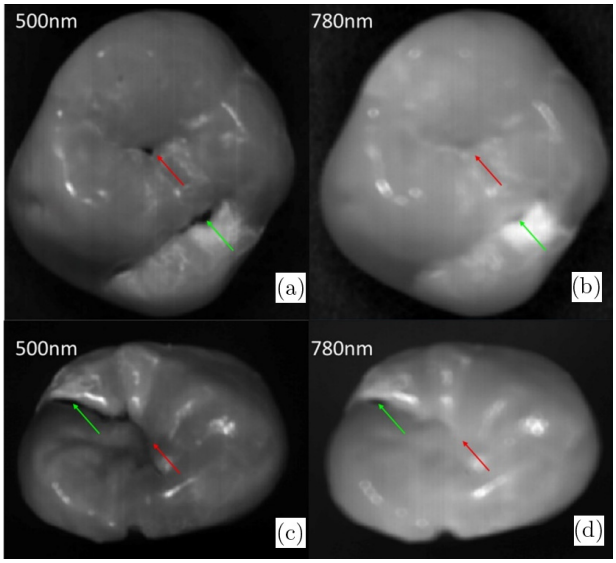

Fig. 10. Tooth images at 500 nm and 780 nm, where (a) and (c) are images of teeth at 500 nm band, and (b) and (d) are images of teeth at 780 nm band, respectively.

when comparing the spectra at different tooth states.

Pigmented black or yellowish-brown teeth film usually adheres to, and deposits on, the surface of the teeth. It is mainly exogenous, including non-metallic substances (food coloring, drinks, tobacco, curry, oral chlorhexidine preparations, drugs entering the mouth, etc.) and metallic substances (nitrates in table salt, iron supplements, copper salts in mouthwashes, etc.).[19] Under white light, it is not possible to distinguish carious lesions from pigmentation with the naked eye or visual inspection.

The main component of the dental enamel is hydroxyapatite, which is about 97% of the total enamel weight.[20] Its crystal structure is hexagonal cylinders, with a width of 40 nm, a thickness of 25 nm and a length of 100–1000 nm. In the enamel, the crystal structure aggregates into prisms, with a width of 4 μm to 6 μm. In addition, the prisms extend from the dentin-enamel junction to the outer surface of the tooth.[21]

The carious surface area appeared whiter than the surface of sound tissue at the waveband of 780 nm, because it could scatter more lights, and the scattered light meets both the Rayleigh scattering and the Mie-scattering.[22] It has also been shown that the light scattering coefficient of normal tooth enamel decreases as the incident light wavelength increases,[23] so that images in the NIR wavebands are brighter and have a higher spectra reflectance than those in the visible wavebands.

The early carious areas have a number of porosities due to effects of demineralization, and the light scattering effect increases in the pores resulting in reduced light reflection,[24] so that the limited optical aperture captures less scattered light and the image has a low brightness characteristic. Light scattering by enamel is attributed to enamel crystallites. Consequently, the backscattered light flux can be related to the size and number of crystallites per unit volume (mineral content).

In the NIR wavebands, the absorption of the pigmented surfaces of the teeth is reduced, presenting mainly as a strong scattering state.[22] The light scattering effect is similar to that of sound surfaces and much less than that of carious areas. Furthermore, in the NIR wavebands, the spectra reflectance overlaps with the tooth surface pigment and is much greater than that of the carious areas.

In summary, in the NIR wavebands, the large number of porosities in the carious areas results in increased scattering and decreased reflection of light. Therefore, the value of reflectance of carious areas is much less than that of sound and pigmented areas. This suggests that the NIR wavebands can distinguish early caries from the pigmented areas.

Most other studies are based on NIR hyperspectral imager (>1000 nm), and focus on quantitative diagnosis of dental caries. In contrast, this study uses the visible-NIR hyperspectral imager (400–1000 nm) to analyze the hyperspectral images to reduce the interference of pigmentation. In addition, the region of interest is extracted and the value of mean is calculated, in order to improve the accuracy.

HSI could accurately locate carious tissue, and assess the corresponding spectral variability. It is essential for the development of reliable clinical diagnostic tools. The automatic classification and visualization algorithms of hyperspectral in sound and carious states have been relatively perfect at present, however, there is still no better classification algorithms to identify pigment from carious lesions.

Based on this foundation, it is expected to guide the oral endoscopy enterprises, or the research of early diagnosis of caries to broaden the ideas and found the NIR wavebands to better respond to the early caries for the R&D of oral endoscopy. This will provide a new idea for the development of diagnosis equipment of early caries.

Conflict of Interest

The authors declare that there are no conflicts of interest relevant to this paper.

Acknowledgment

The research was supported by the National Natural Science Foundation of China 62175153 and the Shanghai Science and Technology Commission 21S902700.

References

1. C. Wang, R. Zhang, Y. Jiang *et al.*, "Fluorescence spectrometry based chromaticity mapping, characterization, and quantitative assessment of dental caries," *Photodiagn. Photodyn. Ther.* **37**, 102711 (2022).
2. M. Abdelaziz, I. Krejci, T. Perneger *et al.*, "Near infrared transillumination compared with radiography to detect and monitor proximal caries: A clinical retrospective study," *J. Dent.* **70**, 40–45 (2018).
3. M. I. G. Ortiz, C. De Melo Alencar, B. L. F. De Paula *et al.*, "Accuracy of near-infrared light transillumination (NILT) compared to bitewing radiograph for detection of interproximal caries in the permanent dentition: A systematic review and meta-analysis," *J. Dent.* **98**, 103351 (2020).
4. C. Wang, H. Qin, G. Lai *et al.*, "Automated classification of dual channel dental imaging of autofluorescence and white lightby convolutional neural networks," *J. Innov. Opt. Heal. Sci.* **5**, 2050014 (2020).
5. G. Lu and B. Fei, "Medical hyperspectral imaging: A review," *J. Biomed. Opt.* **19**(1), 010901 (2014).
6. M. A. Calin, S. V. Parasca, D. Savastru *et al.*, "Hyperspectral imaging in the medical field: Present and future," *Appl. Spectrosc. Rev.* **49**(6), 435–447 (2014).
7. A. U. Rehman, S. A. Qureshi, "A review of the medical hyperspectral imaging systems and unmixing algorithms' in biological tissues," *Photodiagn. Photodyn. Ther.* **33**, 102165 (2021).
8. X. Hu, J. Ou, M. Zhou *et al.*, "Spatial-spectral identification of abnormal leukocytes based on microscopic hyperspectral imaging technology," *J. Innov. Opt. Heal. Sci.* **13**(2), 2050005 (2020).
9. P. Usenik, M. Bürmen, A. Fidler *et al.*, "Near-infrared hyperspectral imaging of water evaporation dynamics for early detection of incipient caries," *J. Dent.* **42**(10), 1242–1247 (2014).
10. Y. H. El-Sharkawy, S. Elbasuney, "Laser induced fluorescence with 2-D Hilbert transform edge detection algorithm and 3D fluorescence images for white spot early recognition," *Spectrochim. Acta A Mol. Biomol. Spectrosc.* **240**, 118616 (2020).
11. Y. H. El-Sharkawy, S. Elbasuney, "Design and implementation of novel hyperspectral imaging for dental carious early detection using laser induced fluorescence," *Photodiagn. Photodyn. Ther.* **24**, 166–178 (2018).
12. A. L. Abdel Gawad, Y. El-Sharkawy, H. S. Ayoub *et al.*, "Classification of dental diseases using hyperspectral imaging and laser induced fluorescence," *Photodiagn. Photodyn. Ther.* **25**, 128–135 (2019).
13. S. C. Chang, H. Y. Syu, Y. L. Wang *et al.*, "Identifying the incidence level of periodontal disease through hyperspectral imaging," *Opt. Quantum Electron.* **50**(11), 1–14 (2018).
14. H. C. Wang, M. T. Tsai, C. P. Chiang, "Visual perception enhancement for detection of cancerous oral tissue by multi-spectral imaging," *J. Opt.* **15** (5), 055301 (2013).
15. D. G. E. Thiem, P. Römer, M. Gielisch *et al.*, "Hyperspectral imaging and artificial intelligence to detect oral malignancy - part 1 - automated tissue classification of oral muscle, fat and mucosa using a light-weight 6-layer deep neural network," *Head Face Med.* **17**(1), 38 (2021).
16. B. E. Urban, H. M. Subhash, "Multimodal hyperspectral fluorescence and spatial frequency domain imaging for tissue health diagnostics of the oral cavity," *Biomed. Opt. Exp.* **12**(11), 6954–6968 (2021).
17. H. C. Wang, Y. T. Chen, "Optimal lighting of RGB LEDs for oral cavity detection," *Opt. Exp.* **20**(9), 10186–10199 (2012).
18. K. H. Cho, C. M. Kang, H. I. Jung *et al.*, "The diagnostic efficacy of quantitative light-induced fluorescence in detection of dental caries of primary teeth," *J. Dent.* **115**, 103845 (2021).
19. J. H. Min, B. R. Kim, B. I. Kim, "Optical detection of the potential for tooth discoloration from children's beverages by quantitative light-induced fluorescence technology," *Photodiagn. Photodyn. Ther.* **34**, 102240 (2021).
20. F. Tetschke, L. Kirsten, J. Golde *et al.*, "Application of optical and spectroscopic technologies for the characterization of carious lesions in vitro," *Biomed. Tech. (Berl).* **63**(5), 595–602 (2018).
21. J. R. Zijp, J. J. ten Bosch, R. A. Groenhuis, "HeNe-laser light scattering by human dental enamel," *J. Dent. Res.* **74**(12), 1891–1898 (1995).
22. J. Vaarkamp, J. J. ten Bosch, E. H. Verdonschot, "Propagation of light through human dental enamel and dentine," *Caries Res.* **29**, 8–13 (1995).
23. D. Fried, R. E. Glena, J. D. Featherstone *et al.*, "Nature of light scattering in dental enamel and

dentin at visible and near-infrared wavelengths," *Appl. Opt.* **34**(7), 1278–1285 (1995).
24. C. M. Zakian, I. A. Pretty, R. Ellwood, "Near-infared hyperspectral imaging of teeth for dental caries detection," *J. Biomed. Opt.* **14**(6), 064047 (2009).